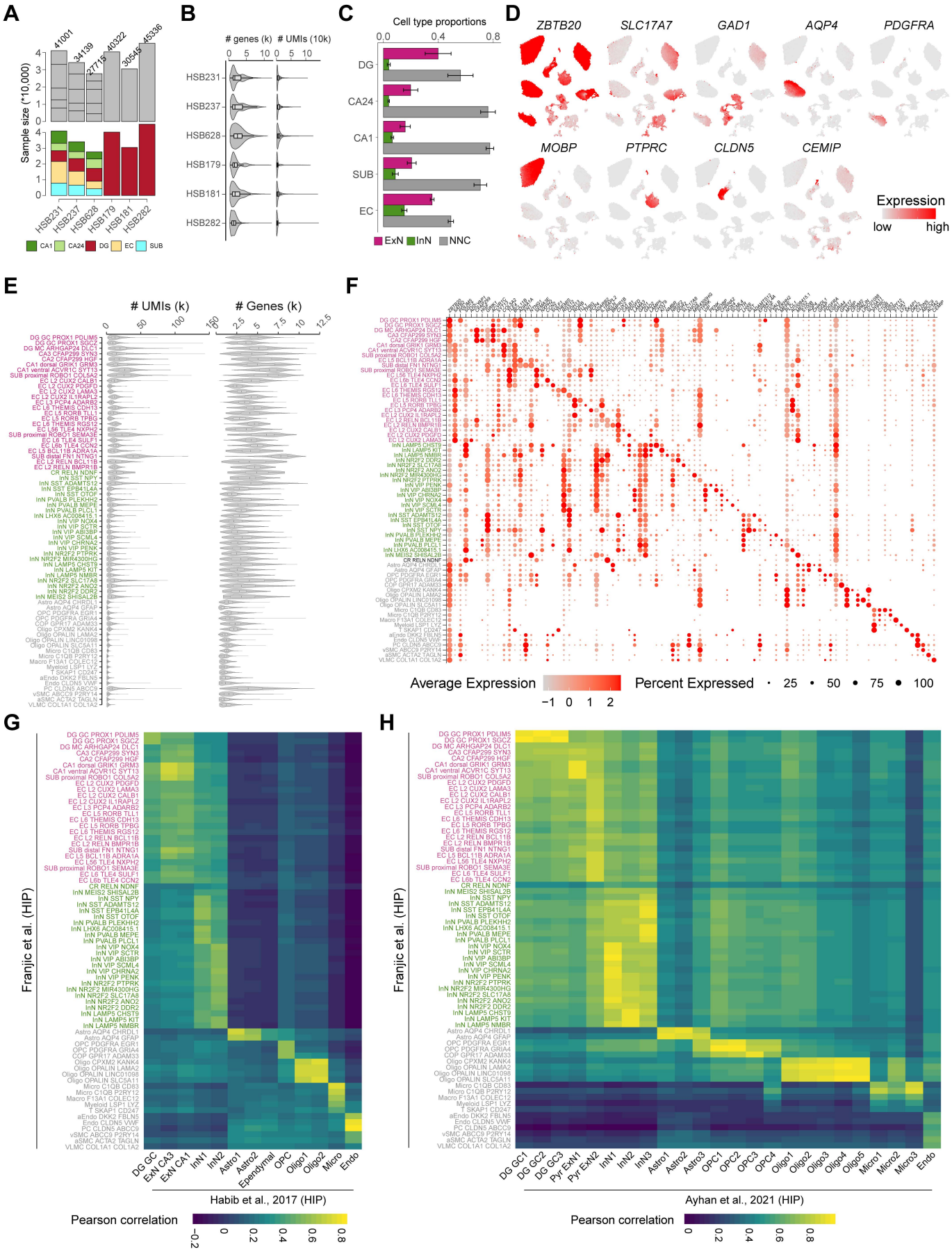
A
B
C
D
E
F
G
H
Sample size (*10,000)
41001
34139
27715
40322
30545
45336
HSB231
HSB237
HSB628
HSB179
HSB181
HSB282
CA1
CA24
DG
EC
SUB
genes (k)
UMIs (10k)
Cell type proportions
ExN
InN
NNC
ZBTB20
SLC17A7
GAD1
AQP4
PDGFRA
MOBP
PTPRC
CLDN5
CEMIP
Expression
low
high
UMIs (k)
Genes (k)
Average Expression
Percent Expressed
Franjic et al. (HIP)
Habib et al., 2017 (HIP)
Ayhan et al., 2021 (HIP)
Pearson correlation

Figure S1 (related to Figure 1). Overview of data quality and preprocessing.
(A) Bar plot showing the number of cells in each donor (x-axis) with segments representing technical replicates (upper panel) and colors denoting subregions (bottom panel).
(B) Violin plot showing the distribution of the number of UMIs and genes detected across donors.
(C) Cell type proportions across regions with error bars representing standard error of mean. Although the overall percentages match the expected ratio of 3 to 1 ExN to InN (DeFelipe et al., 2002; Hodge et al., 2019), we found substantial variations in those proportions between different regions.
(D) UMAP layout visualizing the expression of major cell type markers.
(E) Violin plots displaying the distribution of the number of UMIs and genes across cell subtypes with box plots showing the median, 25th quantiles and 75th quantiles.
(F) Dot plots showing the subtype markers.
(G) Cell types defined in this dataset (y axis) matched to those previously defined in a published hippocampus dataset (Habib et al., 2017) (x axis), where subregions were not selectively dissected.
(H) same as in F, but showing the comparison with the recently published hippocampus data (Ayhan et al., 2021). DG, dentate gyrus; Pyr ExN, pyramidal ExN; EC, entorhinal cortex; Sub, Subiculum. GC, granule cell; MC, mossy cell; Astro, astrocyte; OPC, oligodendrocyte precursor cell; COP, committed oligodendrocyte precursor cell; Oligo, oligodendrocyte; Micro, microglia; Macro, macrophage; Myeloid, myeloid cell; T, T cell; aEndo, arterial endothelial cell; Endo, endothelial cell; PC, pericyte; vSMC, venous smooth muscle cell; aSMC, arterial smooth muscle cell; VLMC, vascular and leptomeningeal cell.

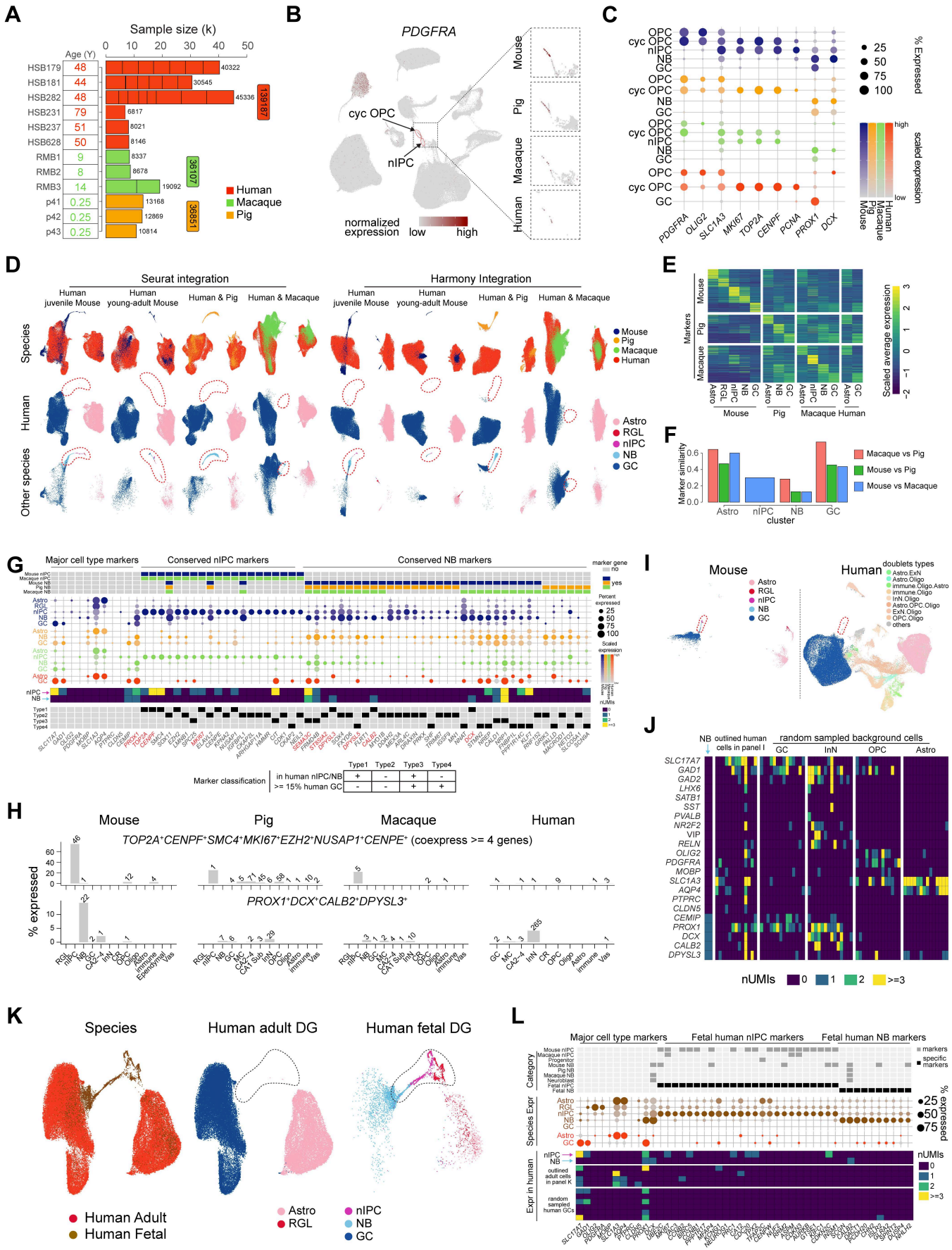
A
Sample size (k)
Age (Y)
HSB179 48 40322
HSB181 44 30545
HSB282 48 45336
HSB231 79 6817
HSB237 51 8021
HSB628 50 8146
RMB1 9 8337
RMB2 8 8678
RMB3 14 19092
p41 0.25 13168
p42 0.25 12869
p43 0.25 10814
136787
36107
36851
Human
Macaque
Pig
B
PDGFRA
cyc OPC
nIPC
normalized expression low high
Mouse
Pig
Macaque
Human
C
OPC
cyc OPC
nIPC
NB
GC
PDGFRA OLIG2 SLC1A3 MKI67 TOP2A CENPF PCNA PROX1 DCX
% Expressed
25 50 75 100
scaled expression
high low
Mouse Pig Macaque Human
D
Seurat integration
Harmony Integration
Human juvenile Mouse
Human young-adult Mouse
Human & Pig
Human & Macaque
Species
Human
Other species
Mouse
Pig
Macaque
Human
Astro
RGL
nIPC
NB
GC
E
Markers
Mouse
Pig
Macaque
Astro RGL nIPC NB GC
Scaled average expression
3 2 1 0 −1 −2
F
Marker similarity
0.6 0.4 0.2 0.0
Macaque vs Pig
Mouse vs Pig
Mouse vs Macaque
Astro nIPC NB GC
cluster
G
Major cell type markers
Conserved nIPC markers
Conserved NB markers
marker gene
no
yes
Percent expressed
25 50 75 100
Scaled expression
nUMIs
Type1 Type2 Type3 Type4
Marker classification
in human nIPC/NB + - + -
>= 15% human GC - - + +
I
Mouse
Astro
RGL
nIPC
NB
GC
Human
doublets types
Astro.ExN
Astro.Oligo
immune.Oligo.Astro
immune.Oligo
InN.Oligo
Astro.OPC.Oligo
ExN.Oligo
OPC.Oligo
others
J
NB outlined human cells in panel I
random sampled background cells
GC InN OPC Astro
SLC17A7
GAD1
GAD2
LHX6
SATB1
SST
PVALB
NR2F2
VIP
RELN
OLIG2
PDGFRA
MOBP
SLC1A3
AQP4
PTPRC
CLDN5
CEMIP
PROX1
DCX
CALB2
DPYSL3
nUMIs 0 1 2 >=3
H
Mouse
Pig
Macaque
Human
TOP2A+CENPF+SMC4+MKI67+EZH2+NUSAP1+CENPE+ (coexpress >= 4 genes)
PROX1+DCX+CALB2+DPYSL3+
% expressed
RGL nIPC NB GC CA2–4 InN CR OPC Oligo Astro immune Ependymal Vas
K
Species
Human adult DG
Human fetal DG
Human Adult
Human Fetal
Astro
RGL
nIPC
NB
GC
L
Major cell type markers
Fetal human nIPC markers
Fetal human NB markers
Category
markers
specific markers
Species Expr
% expressed
25 50 75
Expr in human
nIPC
NB
outlined adult cells in panel K
random sampled human GCs
nUMIs
0 1 2 >=3

Figure S2 (related to Figure 2). Cross-species comparison of hippocampal molecular taxonomy.

(A) Donor ages and sample sizes. Donors are shown on the y-axis and technical replicates are represented by bar segments.

(B) The integration was sensitive enough to identify the cycling oligodendrocyte precursor cells (cyc OPCs), which were close to nIPC domain but marked by a oligodendrocyte precursor marker *PDGFRA*.

(C) Expression of selective OPC, cell cycle markers, as well as *DCX* and *PROX1*, in the granule cell lineage and OPC cells.

(D) Pair-wise integration of astrocytes and granule cell lineage between human and each of the other species using Seurat (left) and Harmony (right). The nIPC and neuroblast domains are outlined.

(E) Scaled average expression of markers across species with rows representing genes and columns denoting cell types.

(F) Similarity of cluster markers measured by the proportion of shared markers.

(G) Expression of species-conserved nIPC and neuroblast markers. Top panel: marker categories. Middle dot plot: expression of the conserved markers across species. Middle heatmap: expression of the markers in the human nIPC and neuroblast. Bottom panel: classification of the markers based on their expression in human neurogenic cells and background granule cells.

(H) Co-expression of type 1 markers identified in panel G across species.

(I) Integration of human and mouse astrocytes and the granule cell lineage along with previously removed human DG doublets.

(J) Expression of major cell type markers and several key neuroblast markers in the human cells outlined in panel I as well as some randomly sampled cells from other cell types. The human neuroblast cell was put on the left for reference.

(K) Integration of adult human DG data and fetal human DG data (Zhong et al., 2020).

(L) Top panel: categories of fetal human markers. Middle panel: expression of these markers in fetal and adult humans. Bottom heatmap: expression of the markers in human with the identified human nIPC and neuroblast arranged on the top for positive controls.

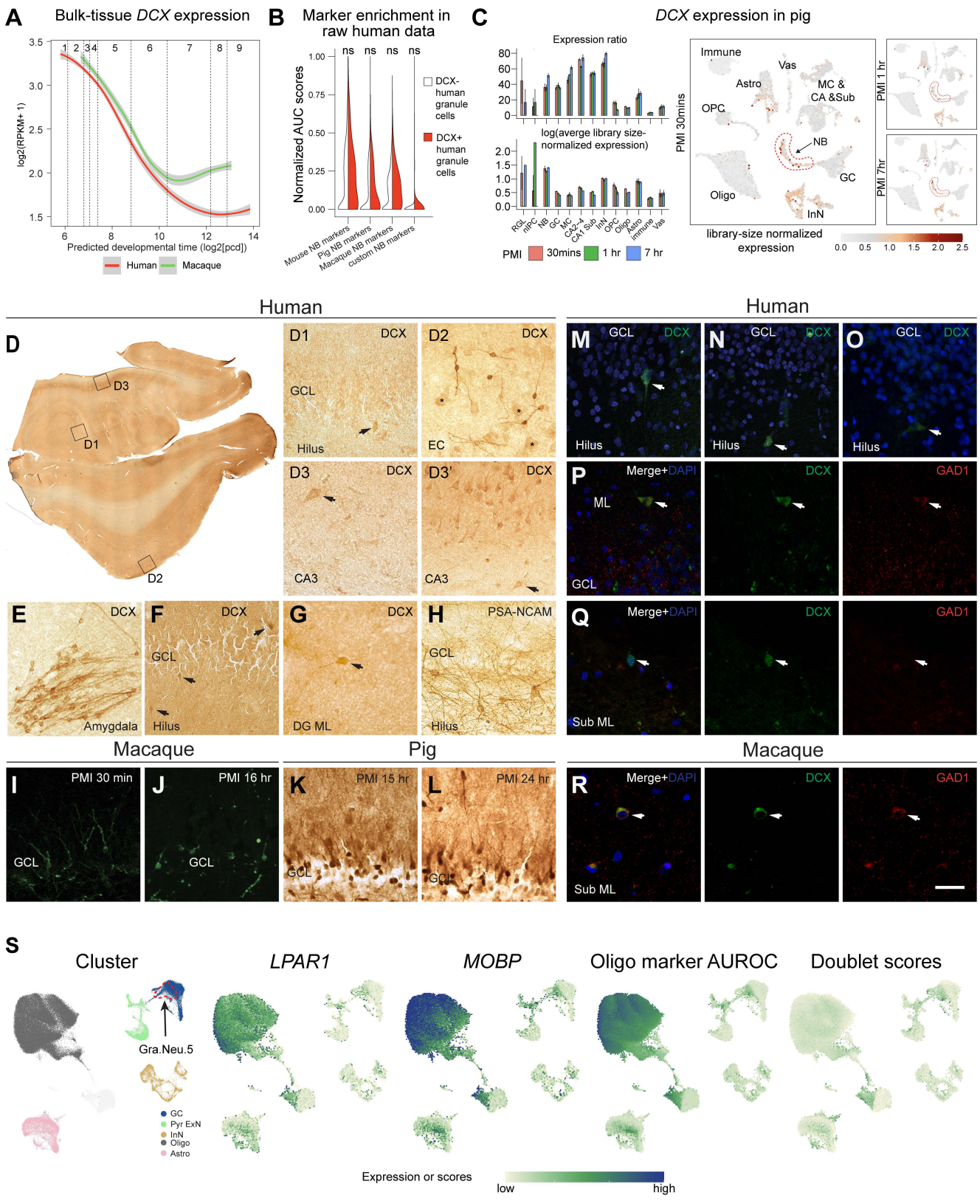
A
Bulk-tissue DCX expression
log2(RPKM+ 1)
Predicted developmental time (log2[pcd])
Human
Macaque
B
Marker enrichment in raw human data
Normalized AUC scores
ns
DCX- human granule cells
DCX+ human granule cells
Mouse NB markers
Pig NB markers
Macaque NB markers
custom NB markers
C
DCX expression in pig
Expression ratio
log(averge library size-normalized expression)
PMI
30mins
1 hr
7 hr
Immune
Vas
Astro
MC & CA &Sub
OPC
NB
GC
Oligo
InN
PMI 30mins
PMI 1 hr
PMI 7hr
library-size normalized expression
Human
Human
D
D1
D2
D3
D3'
Hilus
EC
CA3
DG ML
GCL
DCX
PSA-NCAM
E
Amygdala
F
G
H
M
N
O
P
Q
Merge+DAPI
GAD1
ML
Sub ML
Macaque
Pig
Macaque
I
PMI 30 min
J
PMI 16 hr
K
PMI 15 hr
L
PMI 24 hr
R
S
Cluster
LPAR1
MOBP
Oligo marker AUROC
Doublet scores
Gra.Neu.5
GC
Pyr ExN
InN
Oligo
Astro
Expression or scores
low
high

Figure S3 (related to Figures 3). Cross-species comparison of the *DCX* expression.
(A) Line plots visualizing the expression pattern of *DCX* along the predicted developmental time (Li et al., 2018; Zhu et al., 2018). Dashed lines represent the segregation of nine developmental stages described previously (Li et al., 2018).
(B) Enrichment of different sets of neuroblast markers in *DCX*+ compared to *DCX*- cells in the raw human data prior to down-sampling. Significance was tested using one-tailed Wilcoxon rank sum test (ns: not significant).
(C) Left: Expression ratio and library size normalized expression of *DCX* in pig hippocampus at 30 mins, 1 hour and 7 hours postmortem interval (PMI). Right: UMAP showing normalized expression of *DCX* in pig hippocampus across postmortem intervals.
(D) Panoramic view of the human hippocampus immunolabeled for DCX (DCX-IL) indicating the location of panels D1-D3. D1, DCX-IL dentate gyrus illustrating the lightly labeled cells (arrow) occasionally found around the granule cell layer (GCL). D2, high magnification of the EC layer 2 showing cells clearly immunolabeled by DCX; ghostly, lightly stained cells with pyramidal morphology are marked with asterisks. D3, Lightly DCX-IL cell (arrow) in the stratum oriens of CA3. D3', Same cell (arrow) in the context of other lightly labeled cells in CA3, suggesting possible background staining.
(E) DCX-IL reveals numerous clearly immunoreactive cells in the human amygdala.
(F-G) examples of lightly DCX labeled cells typically located in the hilus, putative SGZ and molecular layer of the DG (arrows).
(H) PSA-NCAM in the human hippocampus labels numerous cells, especially in the hilus of the DG, revealing lack of specificity to label neuroblasts or immature neurons.
(I-L) Effects of PMI on DCX immunolabeling. I, J, DCX-IL cells in the GCL of rhesus macaque after 30 minutes and 16 hours PMI. K, L, DCX-IL cells in the GCL of domestic pig after 15 and 24 hours PMI. Reduced number of DCX-IL cells and increase in dendritic varicosities were observed with increased PMIs, but a sizeable number of cells could be detected. Pig showed occasional cells labeled in the molecular layer and a more immature, less consolidated granule cell layer and numerous cells immunolabeled for DCX in the subgranular zone (SGZ) but also in the hilus, as expected by the young age and the relatively protracted DG development in pigs, as previously described (Guidi et al., 2011).
(M-O) Examples of DCX-IL in the GCL and hilar region of the human.
(P-R) Immunofluorescence labeling of DCX and GAD1 in the hippocampus of human (P, Q) and rhesus macaque (R). Notice colocalization of DCX and GAD1 in one cell (arrow) located in the molecular layer (ML) of the DG of the human (P) and in one cell (arrow) in the molecular layer of the subiculum (Sub ML) of the rhesus (R). Panel Q illustrates a DCX-IL cell located in the Sub ML in the human immunonegative for GAD1. Scale bar represents 2.2 mm in D, 500 µm in D1, 40 µm in D2, 330 µm in D3, 70 µm in D3', 450 µm in E, 800 µm in F, 45 µm in G, 80 µm in H, 50 µm in I and J, 35 µm in K, 50 µm in L, 40 µm in M, 50 µm in N, 35 µm in O, P, 25 µm in Q and 30 µm in R.
(S) From left to right: UMAP visualizing the clusters identified in Ayhan et al., 2021, expression of *LPAR1* and *MOBP* (an oligodendrocyte marker), AUC scores of the top 50 oligodendrocyte markers and the doublet scores. The outlined cell populations represent the "Gra.Neu.5" cluster, which suggested to be a neural progenitor cluster by the original study.

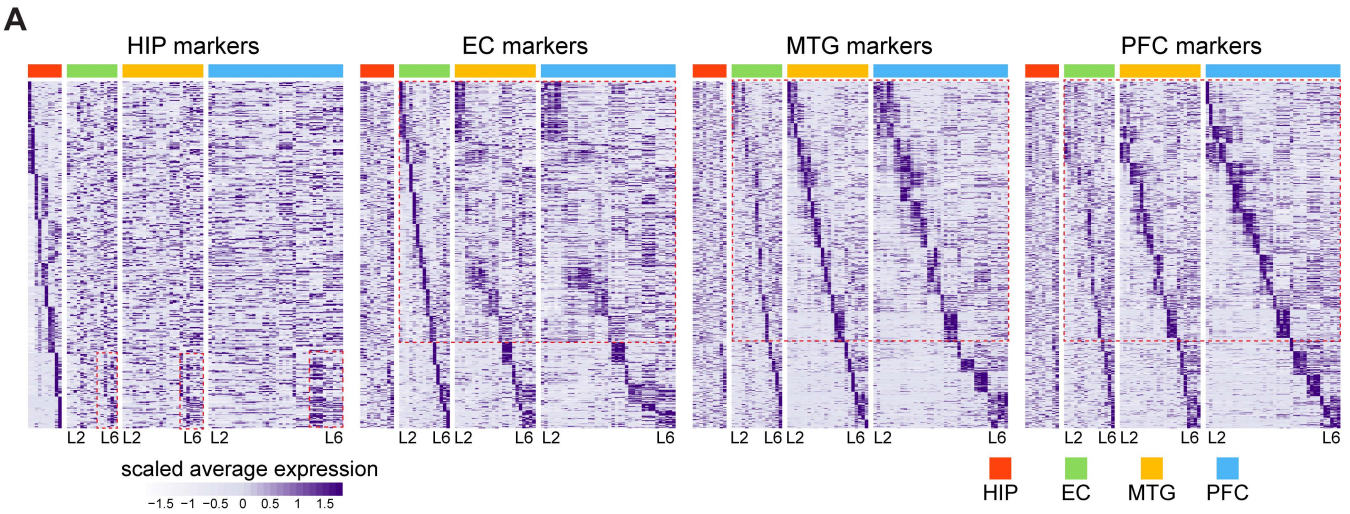

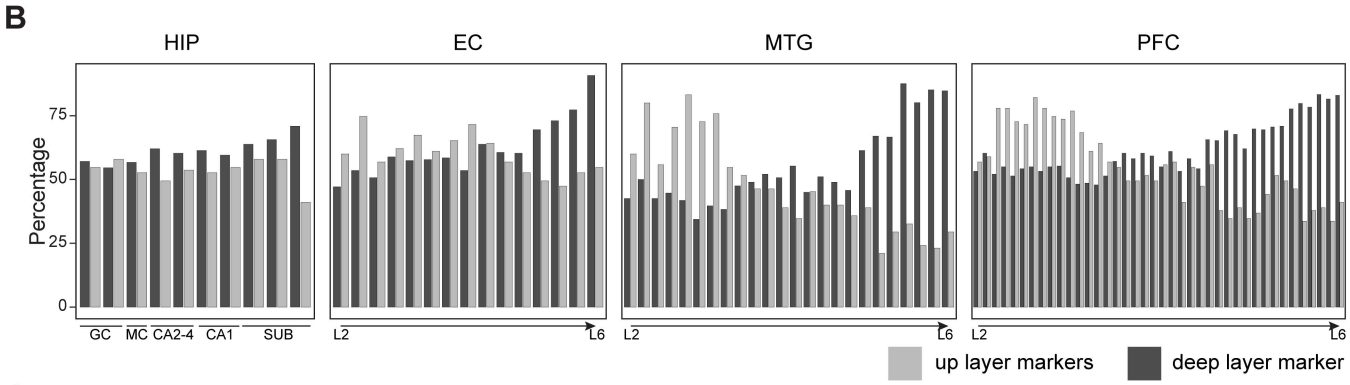

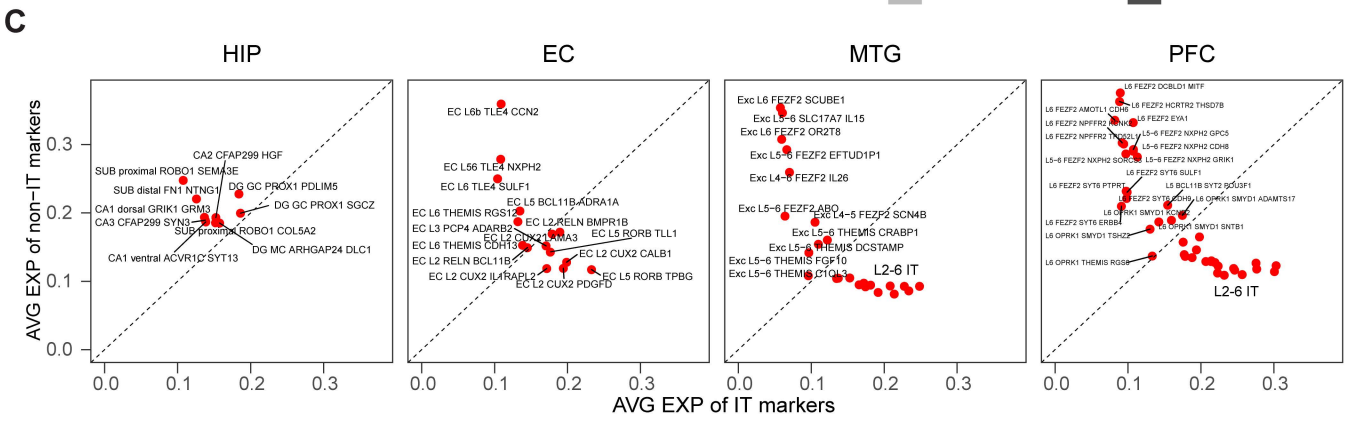

D

# nuclei	Astro AQP4 GFAP	Astro AQP4 CHRDL1
DG	11787	5421
CA2-4	2044	573
CA1	1712	1733
Sub	690	1960
EC	1023	2851

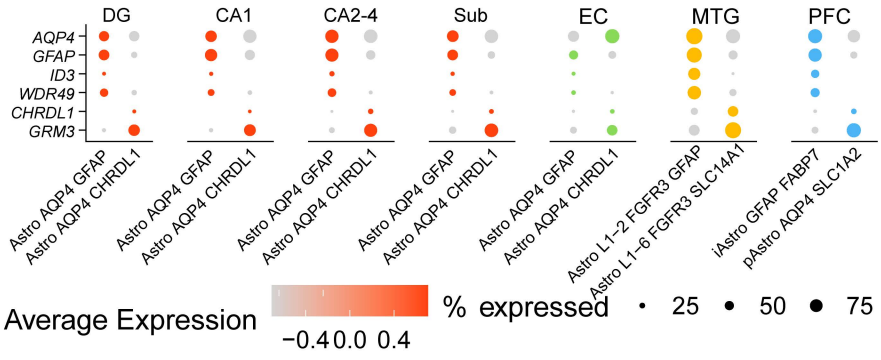

Figure S4 (related to Figure 5). Transcriptome comparison of ExN between hippocampus, EC and neocortex.

(A) Heatmap depicting the expression of marker genes from a certain region (rows) across subtypes (columns) of all the four regions: HIP, EC, MTG and PFC. The relative expression enrichment of hippocampal marker genes in deep layers of EC, MTG and PFC, and the upper layer divergence between EC and neocortex are outlined.

(B) Bar plots denoting the percentages of neocortical upper- (lightgrey) and deep- (black) layer marker genes that were expressed in each subtype of HIP, EC, MTG, and PFC.

(C) Scatter plots showing the average expression of intratelencephalic (IT) neuron markers (x axis) versus that of non-IT markers (y axis) in each subtype of HIP, EC, MTG and PFC.

(D) Left panel: table summarizing the number of cells of each astrocyte subtype across all subregions. Dot plots visualizing the expression of general astrocyte marker (*AQP4*), interlaminar (*GFAP*, *ID3*, *WDR49*) and protoplasmic astrocyte markers (*CHRDL1*, *GRM3*) across all the regions surveyed.

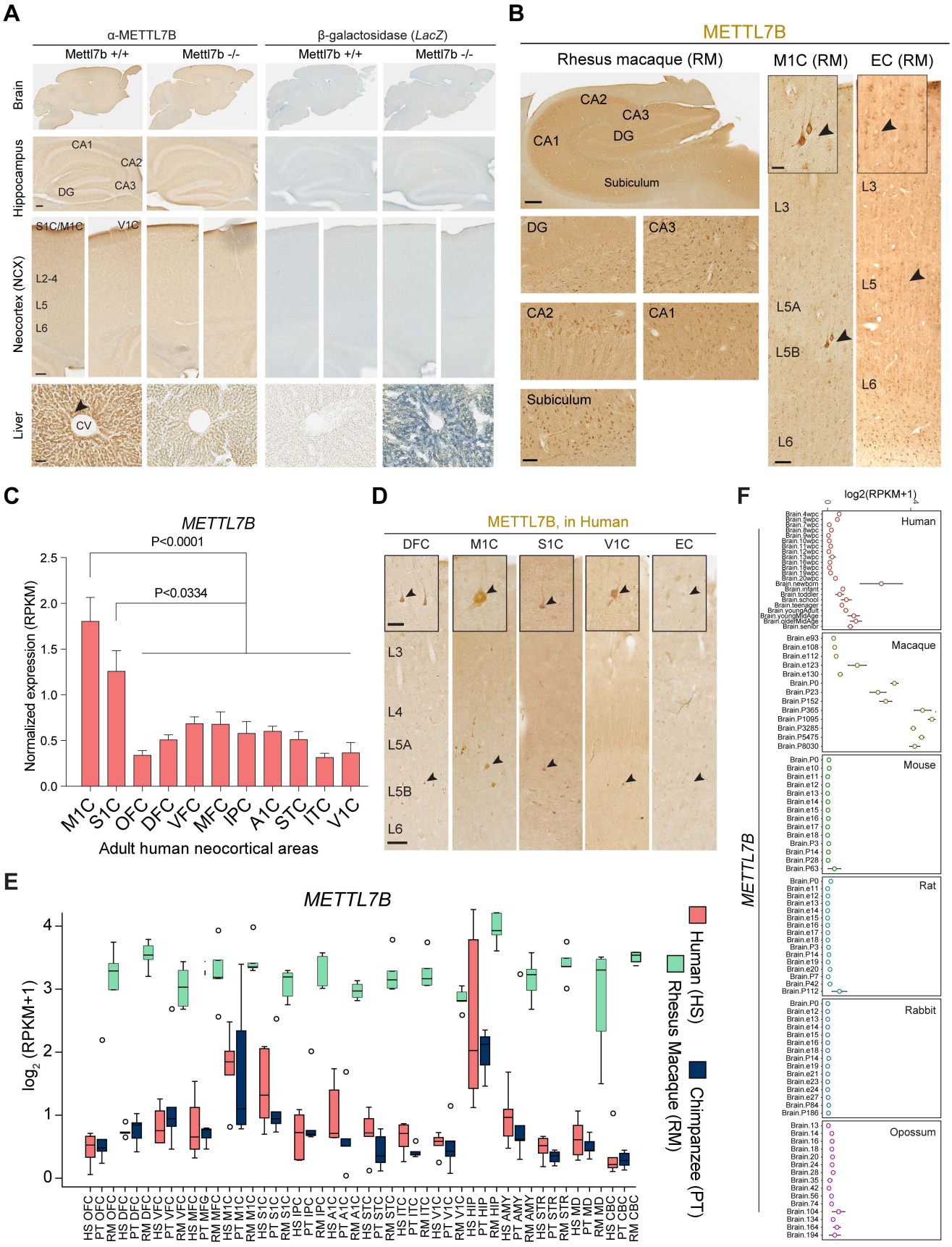
A
α-METTL7B
β-galactosidase (LacZ)
Mettl7b +/+
Mettl7b -/-
Mettl7b +/+
Mettl7b -/-
Brain
Hippocampus
CA1
CA2
CA3
DG
Neocortex (NCX)
S1C/M1C
V1C
L2-4
L5
L6
Liver
CV
B
METTL7B
Rhesus macaque (RM)
M1C (RM)
EC (RM)
CA2
CA3
CA1
DG
Subiculum
DG
CA3
CA2
CA1
Subiculum
L3
L5A
L5B
L6
L3
L5
L6
C
METTL7B
P<0.0001
P<0.0334
Normalized expression (RPKM)
2.5
2.0
1.5
1.0
0.5
0.0
M1C
S1C
OFC
DFC
VFC
MFC
IPC
A1C
STC
ITC
V1C
Adult human neocortical areas
D
METTL7B, in Human
DFC
M1C
S1C
V1C
EC
L3
L4
L5A
L5B
L6
E
METTL7B
log2 (RPKM+1)
4
3
2
1
0
HS OFC
PT OFC
RM OFC
HS DFC
PT DFC
RM DFC
HS VFC
PT VFC
RM VFC
HS MFC
PT MFG
RM MFC
HS M1C
PT M1C
RM M1C
HS S1C
PT S1C
RM S1C
HS IPC
PT IPC
RM IPC
HS A1C
PT A1C
RM A1C
HS STC
PT STC
RM STC
HS ITC
PT ITC
RM ITC
HS V1C
PT V1C
RM V1C
HS HIP
PT HIP
RM HIP
HS AMY
PT AMY
RM AMY
HS STR
PT STR
RM STR
HS MD
PT MD
RM MD
HS CBC
PT CBC
RM CBC
Human (HS)
Chimpanzee (PT)
Rhesus Macaque (RM)
F
log2(RPKM+1)
METTL7B
Human
Brain.4wpc
Brain.5wpc
Brain.7wpc
Brain.8wpc
Brain.9wpc
Brain.10wpc
Brain.11wpc
Brain.12wpc
Brain.13wpc
Brain.16wpc
Brain.18wpc
Brain.19wpc
Brain.20wpc
Brain.newborn
Brain.infant
Brain.toddler
Brain.school
Brain.teenager
Brain.youngAdult
Brain.youngMidAge
Brain.olderMidAge
Brain.senior
Macaque
Brain.e93
Brain.e108
Brain.e112
Brain.e123
Brain.e130
Brain.P0
Brain.P23
Brain.P152
Brain.P365
Brain.P1095
Brain.P3285
Brain.P5475
Brain.P8030
Mouse
Brain.P0
Brain.e10
Brain.e11
Brain.e12
Brain.e13
Brain.e14
Brain.e15
Brain.e16
Brain.e17
Brain.e18
Brain.P3
Brain.P14
Brain.P28
Brain.P63
Rat
Brain.P0
Brain.e11
Brain.e12
Brain.e13
Brain.e14
Brain.e15
Brain.e16
Brain.e17
Brain.e18
Brain.P3
Brain.P14
Brain.e19
Brain.e20
Brain.P7
Brain.P42
Brain.P112
Rabbit
Brain.P0
Brain.e12
Brain.e13
Brain.e14
Brain.e15
Brain.e16
Brain.e18
Brain.P14
Brain.e19
Brain.e21
Brain.e23
Brain.e24
Brain.e27
Brain.P84
Brain.P186
Opossum
Brain.13
Brain.14
Brain.16
Brain.18
Brain.20
Brain.24
Brain.28
Brain.35
Brain.42
Brain.56
Brain.74
Brain.104
Brain.134
Brain.164
Brain.194

Figure S5 (related to Figure 6). *METTL7B* is expressed in human and macaque brain but not mouse and pig brain.

(A) Immunostaining of Mettl7b protein and lacZ expression in brain and liver. No expression was observed in the adult mouse brain. Scale bars: brain = 100 μm; liver = 50 μm. CV = central vein.

(B) METTL7B immunolabeling of hippocampus, primate motor cortex and EC in rhesus macaque brains. Note labeling of hippocampal neurons, Betz cells, and pyramidal neurons in EC. Scale bars = 100 μm; inset = 50 μm.

(C) RNA-seq expression of *METTL7B* in human neocortex. One-way ANOVA with post-hoc Dunnett's adjustment, all groups n=6, except MFC n=5. Data are means ± SEM.

(D) Prominent immunolabeling of layer 5B (L5B) pyramidal neurons (arrowheads), including Betz and Meynert cells in M1C and V1C, respectively. Scale bars = 150 μm; insets = 50 μm.

(E) RNA-seq expression of *METTL7B* homologs in human, chimpanzee, and rhesus macaque brain regions (Sousa et al., 2017).

(F) RNA-seq expression of *METTL7B* in the brain (forebrain/cerebrum) of multiple species at different developmental stages. Expression data was obtained from Cardoso-Moreira et al. 2019. AMY, amygdala; A1C, primary auditory cortex; CBC, cerebellar cortex; DFC, dorsolateral prefrontal cortex (aka DLPFC); EC, entorhinal cortex; IPC, posterior inferior parietal cortex; ITC, inferior temporal cortex M1C, primary motor cortex; MD, mediodorsal nucleus of the thalamus; MFC, medial prefrontal cortex; OFC, orbital prefrontal cortex; S1C, primary somatosensory cortex; STC, superior temporal cortex; STR, striatum; V1C, primary visual cortex; VFC, ventrolateral prefrontal cortex.

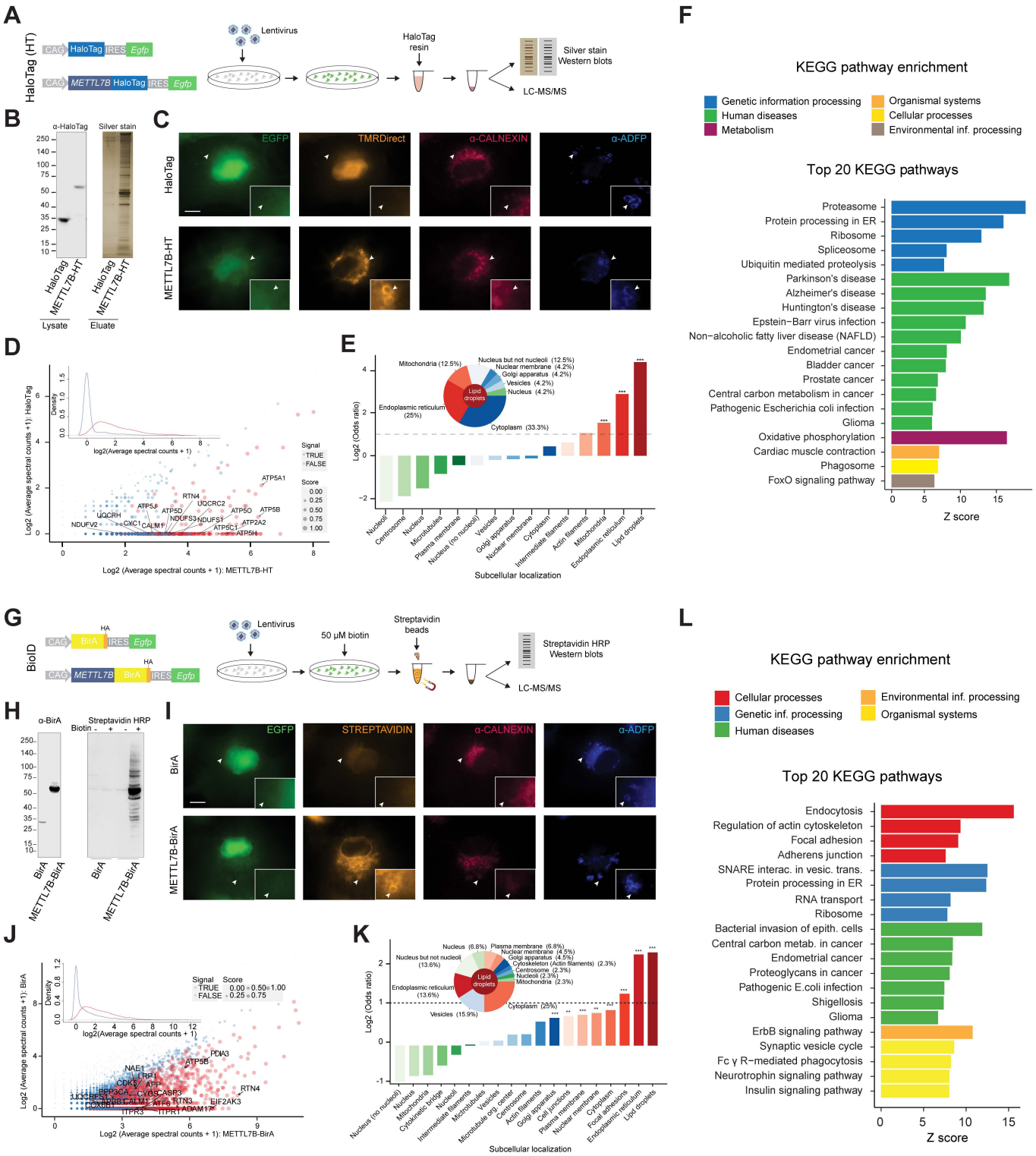
A
HaloTag (HT)
CAG HaloTag IRES Egfp
CAG METTL7B HaloTag IRES Egfp
Lentivirus
HaloTag resin
Silver stain
Western blots
LC-MS/MS
B
α-HaloTag
Silver stain
250
140
100
75
50
40
35
25
15
10
HaloTag
METTL7B-HT
Lysate
Eluate
C
EGFP
TMRDirect
α-CALNEXIN
α-ADFP
HaloTag
METTL7B-HT
D
Log2 (Average spectral counts + 1): HaloTag
Log2 (Average spectral counts + 1): METTL7B-HT
log2(Average spectral counts + 1)
Density
Signal
TRUE
FALSE
Score
ATP5A1
RTN4
UQCRC2
ATP5J
ATP5D
ATP5O
ATP5B
UQCRH
NDUFS3
NDUFS1
ATP2A2
NDUFV2
CXC1
CALM1
ATP5C1
ATP5H
E
Log2 (Odds ratio)
Mitochondria (12.5%)
Nucleus but not nucleoli (12.5%)
Nuclear membrane (4.2%)
Golgi apparatus (4.2%)
Vesicles (4.2%)
Nucleus (4.2%)
Lipid droplets
Endoplasmic reticulum (25%)
Cytoplasm (33.3%)
Nucleoli
Centrosome
Nucleolus
Microtubules
Plasma membrane
Nucleus (no nucleoli)
Vesicles
Golgi apparatus
Nuclear membrane
Cytoplasm
Intermediate filaments
Actin filaments
Mitochondria
Endoplasmic reticulum
Lipid droplets
Subcellular localization
F
KEGG pathway enrichment
Genetic information processing
Human diseases
Metabolism
Organismal systems
Cellular processes
Environmental inf. processing
Top 20 KEGG pathways
Proteasome
Protein processing in ER
Ribosome
Spliceosome
Ubiquitin mediated proteolysis
Parkinson's disease
Alzheimer's disease
Huntington's disease
Epstein−Barr virus infection
Non−alcoholic fatty liver disease (NAFLD)
Endometrial cancer
Bladder cancer
Prostate cancer
Central carbon metabolism in cancer
Pathogenic Escherichia coli infection
Glioma
Oxidative phosphorylation
Cardiac muscle contraction
Phagosome
FoxO signaling pathway
Z score
G
BioID
HA
CAG BirA IRES Egfp
CAG METTL7B BirA IRES Egfp
Lentivirus
50 μM biotin
Streptavidin beads
Streptavidin HRP
Western blots
LC-MS/MS
H
α-BirA
Streptavidin HRP
Biotin
250
140
100
75
50
40
35
25
15
10
BirA
METTL7B-BirA
I
EGFP
STREPTAVIDIN
α-CALNEXIN
α-ADFP
BirA
METTL7B-BirA
J
Log2 (Average spectral counts + 1): BirA
Log2 (Average spectral counts + 1): METTL7B-BirA
log2(Average spectral counts + 1)
Density
Signal
TRUE
FALSE
Score
PDA3
ATP5B
NAE1
LRP1
CDK5
ATP5
PPP3CA
CYB5R3
RTN4
UQCRC1
UQCRB
CALM1
ATP5
RTN3
EIF2AK3
ITPR3
ITPR1
ADAM17
K
Log2 (Odds ratio)
Nucleus (6.8%)
Plasma membrane (6.8%)
Nucleus but not nucleoli (13.6%)
Nuclear membrane (4.5%)
Golgi apparatus (4.5%)
Cytoskeleton (Actin filaments) (2.3%)
Centrosome (2.3%)
Nucleoli (2.3%)
Mitochondria (2.3%)
Lipid droplets
Endoplasmic reticulum (13.6%)
Vesicles (15.9%)
Cytoplasm (25%)
Nucleus (no nucleoli)
Nucleolus
Mitochondria
Cytoskeletal bridge
Nucleoli
Intermediate filaments
Microtubules
Vesicles
Microtubule org. center
Centrosome
Actin filaments
Golgi apparatus
Cell junctions
Plasma membrane
Nuclear membrane
Cytoplasm
Focal adhesions
Endoplasmic reticulum
Lipid droplets
Subcellular localization
L
KEGG pathway enrichment
Cellular processes
Genetic inf. processing
Human diseases
Environmental inf. processing
Organismal systems
Top 20 KEGG pathways
Endocytosis
Regulation of actin cytoskeleton
Focal adhesion
Adherens junction
SNARE interac. in vesic. trans.
Protein processing in ER
RNA transport
Ribosome
Bacterial invasion of epith. cells
Central carbon metab. in cancer
Endometrial cancer
Proteoglycans in cancer
Pathogenic E.coli infection
Shigellosis
Glioma
ErbB signaling pathway
Synaptic vesicle cycle
Fc γ R−mediated phagocytosis
Neurotrophin signaling pathway
Insulin signaling pathway
Z score

Figure S6 (related to Figure 7). KEGG pathway enrichment of METTL7B interacting proteins.

(A) Schematic of HaloTag (HT) pulldown design.

(B) Immunoblot validation of HT proteins and silver stain of pulldown eluates showing more proteins captured in METTL7B-HT sample.

(C) Immunofluorescence staining showing that METTL7B fusion protein (TMR-Direct) co-localizes with CALNEXIN and ADFP, markers of the ER and LD, respectively (Turro et al., 2006). Scale bars = 10 μm

(D) SAINT analysis distinguishes true METTL7B interactors (red) from false ones (blue) based on MS spectral counts. The figure shows the average spectral counts in 3 test experiments (x axis) and 3 control experiments for all detected proteins. The inset clarifies separation between true METTL7B interactors (red curve) and the false ones (blue curve) in terms of spectral count distribution.

(E) Fold-enrichment test for major subcellular compartments cataloged in Human Protein Atlas database (Uhlen et al., 2015) and mammalian cytoplasmic lipid droplet proteomes (Hodges and Wu, 2010). The inset shows subcellular composition (%) of LD associated proteins. ***P<0.001.

(F) KEGG pathway enrichment analysis showing molecular pathways involving true interactors are associated with three neurodegenerative diseases: Alzheimer's, Parkinson's, and Huntington's disease.

(G) Schematic of BioID pulldown experimental design.

(H) Immunoblot validation of BioID proteins (α-BirA) and pulldown efficiency (STREPTAVIDIN-HRP) after supplementing cell culture media with 50 μM biotin for 24 hours.

(I) METTL7B-expressing cells exhibit vast biotinylation of endogenous proteins (STREPTAVIDIN) which co-localize with CALNEXIN and ADFP, ER and LD markers, respectively. Scale bars = 10 μm

(J) SAINT analysis distinguishes true METTL7B interactors (red) from false ones (blue) based on MS spectral counts. The figure shows the average spectral counts in 3 test experiments (x axis) and 3 control experiments for all detected proteins. The inset clarifies separation between true METTL7B interactors (red curve) and the false ones (blue curve) in terms of spectral count distribution.

(K) Fold-enrichment test for major subcellular compartments cataloged in Human Protein Atlas database (Uhlen et al., 2015) and mammalian cytoplasmic lipid droplet proteomes (Hodges and Wu, 2010). The inset shows subcellular composition (%) of LD associated proteins. ***P<0.001, **P<0.01.

(L) KEGG pathway enrichment analysis.

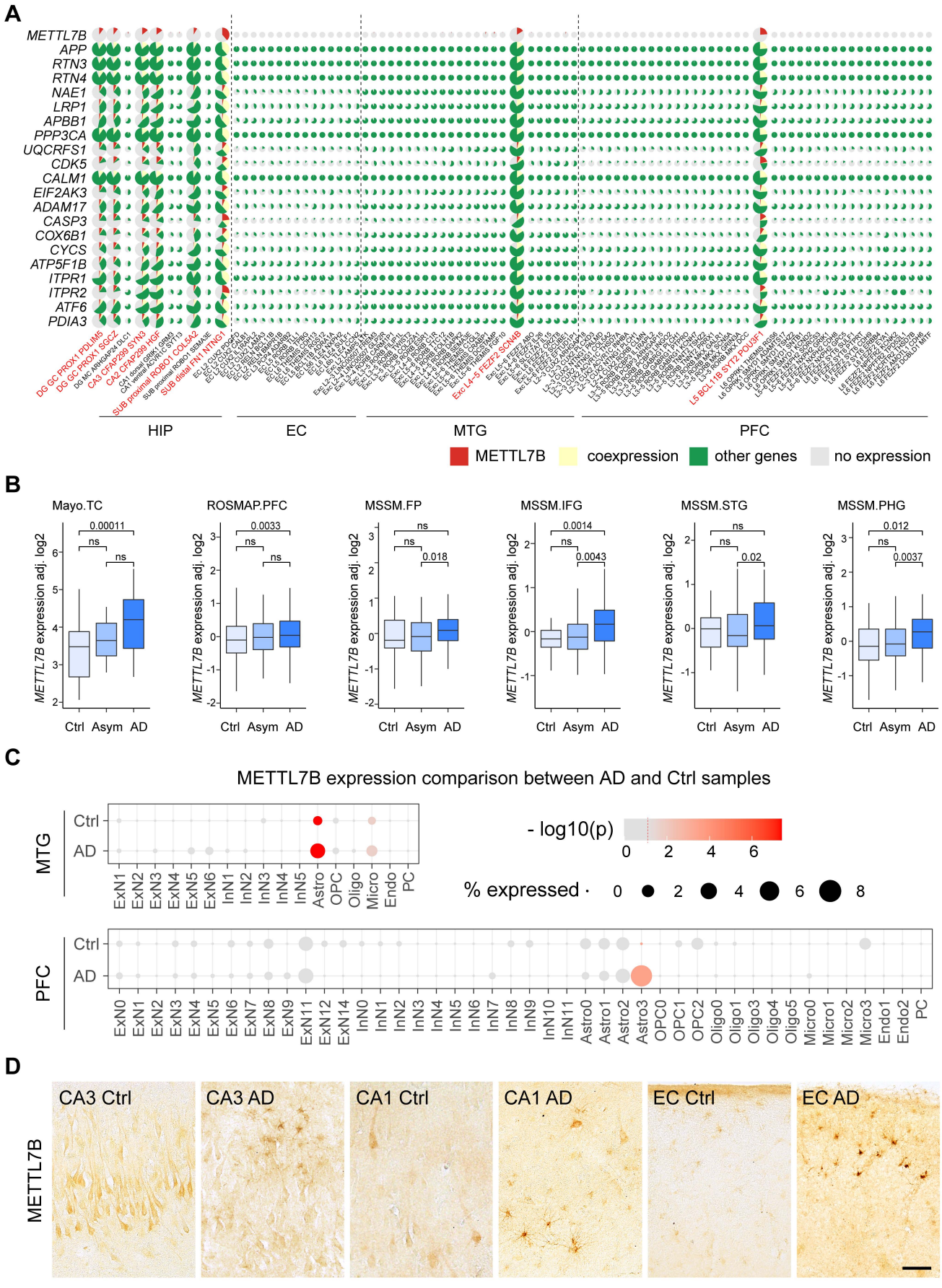
A
METTL7B
APP
RTN3
RTN4
NAE1
LRP1
APBB1
PPP3CA
UQCRFS1
CDK5
CALM1
EIF2AK3
ADAM17
CASP3
COX6B1
CYCS
ATP5F1B
ITPR1
ITPR2
ATF6
PDIA3
HIP
EC
MTG
PFC
METTL7B
coexpression
other genes
no expression
B
Mayo.TC
ROSMAP.PFC
MSSM.FP
MSSM.IFG
MSSM.STG
MSSM.PHG
METTL7B expression adj. log2
Ctrl
Asym
AD
0.00011
0.0033
0.018
0.0014
0.0043
0.02
0.012
0.0037
ns
C
METTL7B expression comparison between AD and Ctrl samples
MTG
PFC
Ctrl
AD
- log10(p)
% expressed
ExN0
ExN1
ExN2
ExN3
ExN4
ExN5
ExN6
ExN7
ExN8
ExN9
ExN11
ExN12
ExN14
InN0
InN1
InN2
InN3
InN4
InN5
InN6
InN7
InN8
InN9
InN10
InN11
Astro0
Astro1
Astro2
Astro3
OPC0
OPC1
OPC2
Oligo0
Oligo1
Oligo3
Oligo4
Oligo5
Micro0
Micro1
Micro2
Micro3
Endo1
Endo2
PC
D
METTL7B
CA3 Ctrl
CA3 AD
CA1 Ctrl
CA1 AD
EC Ctrl
EC AD

Figure S7 (related to Figure 7). *METTL7B* expression in control and Alzheimer's disease brains.

(A) Pie charts showing the percent of cells expressing *METTL7B* but not certain *METTL7B* interactor (red), the percent of cells expressing each of the *METTL7B* interactors but not *METTL7B* (green), as well as the percent of cells co-expressing *METTL7B* and certain interactor (yellow) out of all cells within the subtypes of HIP, EC, MTG and PFC. Each row represents a gene and each column denotes a subtype.

(B) *METTL7B* expression from bulk tissue RNA-seq of control (Ctrl), asymptomatic AD (Asym), and AD from several brain regions. TC, temporal cortex; PFC, prefrontal cortex; FP, frontal pole; IFG, inferior frontal gyrus; STG, superior temporal gyrus; PHG, parahippocampal gyrus. Data analyzed from Swarup Lab (http://swaruplab.bio.uci.edu:3838/bulkRNA/).

(C) Expression of *METTL7B* across cell types from Ctrl and AD brains. The sizes of dots represent the expression ratio of METTL7B and the color gradients represent significance of METTL7B enriched in AD subtypes (measured by Fisher's exact test, two-sided). All dots with p value smaller than 0.05 are colored in red gradients. Top: prefrontal cortex (Mathys et al., 2019). Bottom: middle temporal cortex (**STAR Methods**).

(**D)** Immunostaining of METTL7B in CA3, CA1 and EC in both control and AD brains. Scale bar is 60 μm for all panels. Astro, astrocyte; OPC, oligodendrocyte progenitor cell; Oligo, oligodendrocyte; Micro, microglia; Endo, endothelial cell; PC, pericyte.